

# Minimally Intrusive Single-Chip Recession/Temperature Sensors for Spacecraft Thermal Protection Systems

Robert Okojie  
NASA Glenn Research Center  
21000 Brookpark Road  
Cleveland, OH 44135  
Robert.S.Okojie@nasa.gov

Gary Go  
Innoveering, Inc  
61 Keyland Ct  
Bohemia, NY 11716  
Gary.Go@Innoveering.net

Christian Petrov  
Innoveering, Inc  
61 Keyland Ct  
Bohemia, NY 11716  
Christian.Petrov@Innoveering.net

Nick Tiliakos  
Innoveering, Inc  
61 Keyland Ct  
Bohemia, NY 11716  
Nick.Tiliakos@Innoveering.net

**Abstract**— We report the initial results of ongoing development of minimally intrusive, single-chip integrated capacitive recession/temperature sensors that would provide real-time monitoring of ablation recession of heatshield thermal protection systems (TPS) during spacecraft atmospheric entry. This work, which was performed using Phenolic Impregnated Carbon Ablator (PICA), is also to demonstrate the ease of sensor insertion during TPS manufacturing, thereby resulting in faster, low-cost, uniform sensor assembly, and spatial distribution, without compromising TPS structural integrity. Using oxy-acetylene flame at 500 W-cm<sup>-2</sup> heat flux for 16 seconds, the average recession depth of 0.325 cm was obtained. While some measurement challenges were encountered in this first attempt, the initial results obtained were in relatively good agreement with published data, which offer promise of future improvement based on lessons learned.

## Table of Contents

1. INTRODUCTION.....	1
2. SENSING PRINCIPLES .....	2
3. SENSOR FABRICATION AND PREPARATION .....	3
4. TEST SETUP AND CALIBRATION .....	3
5. SENSOR TESTING.....	4
6. RESULTS AND DISCUSSION.....	5
7. CONCLUSION .....	6
ACKNOWLEDGEMENTS .....	6
REFERENCES.....	6
BIOGRAPHY .....	7

## 1. INTRODUCTION

The safety and overall mission success of space vehicles rely heavily on the integrity of the TPS to protect valuable payloads and humans during atmospheric entry. Future missions would comprise of humans, life supporting

infrastructures, and robotic builders. Therefore, it is imperative to monitor the health of the TPS sufficiently and efficiently by way of large area coverage of the surface with miniature, low weight, and minimally intrusive instrumentation.

Previous studies estimated that the payload could be as large as 80 mt while the entry mass could be three times higher [1-4], resulting in higher energy entry. This implies that the recession rate of the TPS material must be adequately quantified at a higher fidelity beyond the current state of the art (SoA) 2020 Mars Science Laboratory Entry Descent and Landing Instrumentation (MEDLI-2) [5]. TPS thickness optimization would result in a significant mass reduction of the entry vehicle, thereby reducing \$/lb launch cost and retaining of payload weight. This is with the goal of achieving the prescribed 50% mass reduction.

Many elements of Entry, Descent, and Landing (EDL) cannot be replicated in ground test facilities, either due to Earth-based limitations (gravity, gas composition, etc.) or due to practicalities achieving the appropriate high energy flows. Hence, heavy dependence is placed on aerothermal modeling and simulation. However, the uncertainties that exist in these simulations make the need for experimental validation more critical [6, 7]. The data obtained from these tests would help to validate and improve the aerothermal and aerodynamic codes that are used in the modeling and simulation of atmospheric entry effects on TPS. In addition, this work is intended to advance the development of high fidelity and real-time health monitoring of vehicle TPS during atmospheric entry; to demonstrate ease of sensor insertion during TPS manufacture, without compromising its structural integrity; increase sensor spatial distribution across TPS surface to provide global monitoring of TPS during high mass entry. It is also intended to enable TPS thickness optimization, thereby enabling system-level risk balancing during mission design. The net result will be future missions with increased reliability and improved mass and volume

### Notice for Copyrighted Information

This manuscript is a joint work of employees of the National Aeronautics and Space Administration and employees of Innoveering, Inc., under Contract No. 80NSSC18P1437 with the National Aeronautics and Space Administration. The United States Government may prepare derivative works, publish, or reproduce this manuscript and allow others to do so. Any publisher accepting this manuscript for publication acknowledges that the United States Government retains a non-exclusive, irrevocable, worldwide license to prepare derivative works, publish, or reproduce the published form of this manuscript, or allow others to do so, for United States government purposes.

ratios of payload to spacecraft.

As represented in Figs. 1a and b, the MEDLI-2 used similar TPS plugs instrumented with thermocouples (TC's) to measure depth-resolved thermal response from which recession rate could be inferred [8]. The plug-in configuration evolved from the successful MEDLI-1 mission. As seen in Fig. 1b, eleven of these PICA plugs were used, each

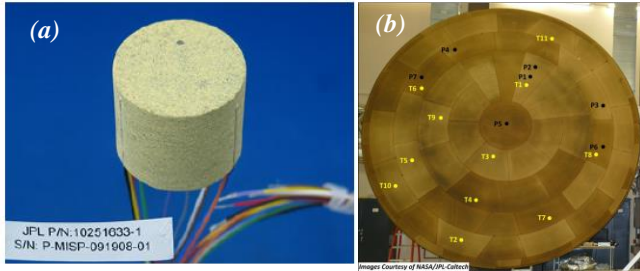


**Fig. 1: a) Instrumented PICA plug that is representative of the plugs used in b) Mars 2020 TPS, showing locations of plugs [8].**

containing depth resolved TC's to measure in-depth thermal response. Such plug-in instrumentation scheme required mating cylindrical holes to be drilled out of the main TPS body. Only limited number of holes could be drilled, taking cognizance of the need to maintain the structural integrity of the heatshield material. As a result of such limitation, the effective aerothermal measurements that are captured during entry are only confined to areas vicinal to the plugs. Another important issue worth considering is that when the instrumented plug is mated into the hole, the circumferential gap is filled with a bonding material, which leaves an annular bond-line that could become a potential nucleation site for localized aero shocks and non-uniform ablation during high mass entry. Also, the fidelity of the recession rate is low because the four varied depth placement of the TC's do not provide continuous ablation/recession measurement. Therefore, the recession rate obtained would not provide an effective solution for TPS thickness optimization used in future high mass entry vehicles.

The demonstration of several atmospheric recession sensing strategies (i.e., capacitive, resistive, acoustic, and optical) have been previously reported [9-11]. However, they suffer from some common or unique drawbacks that included large size (large form factor), inconsistent placement due to manual assembly, low sensitivity and fidelity, and reproducibility of results.

The work reported here leveraged the advantages of batch microfabrication techniques to implement single-chip MEMS-based integrated capacitive recession sensors and resistor thermal detectors (RTD's) on a semi-insulating silicon carbide (SiC) substrate. The size of each integrated sensors suite was 500  $\mu\text{m}$  thick, 1.93 cm wide, and 2.55 cm long. When used only as a discrete capacitive recession sensor, the width was 0.2 cm. As a result, only a tiny hole of slightly larger dimension than the recession sensor was needed to be drilled into the main TPS body. The sensor could then be slid into the tiny hole, thereby avoiding the need for drilling large  $> 2.54$  cm diameter holes as was done in MEDLI [8]. This approach overcomes the several

disadvantages of previous methods reported in literature, as well as to provide real-time, high resolution recession rate and temperature sensing capability.

The MEMS-based integrated capacitive recession sensor /RTD is shown in the mask layout illustration of Fig. 2a. The left-most rectangular feature is the 0.2 cm wide capacitive recession sensor, which is shown in a cross section view in Fig. 2b. The remaining features to the right of the recession sensor are the four RTD's that are precisely placed at varying depth. Due to some design oversight relating to the RTD, this report would present only the results from the discrete capacitive recession sensor.

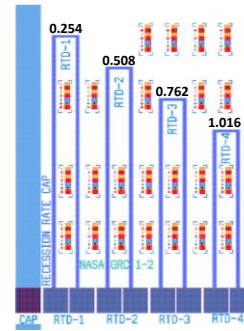


**Fig. 2a: Mask layout of the integrated capacitive recession and temperature sensors chip. Denoted are the depths of the RTDs in the PICA sample (cm).**

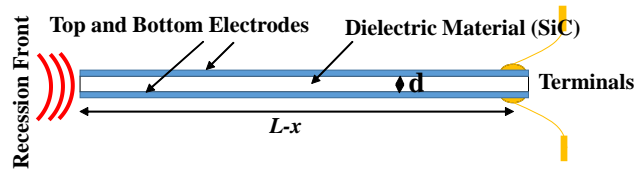


**Fig. 2b: Illustrative cross section rendition of the capacitive recession sensor.**

## 2. SENSING PRINCIPLES

During ablation, the resistors would simultaneously measure the depth-resolved temperature gradients in the TPS, with the longest RTD that is 0.254 cm from the virgin TPS surface measuring the highest temperature near the ablation front before tripping to an open circuit. Simultaneously, the RTD located at 1.016 cm from the surface would record the lowest temperature. This results in a measured and recorded transient temperature gradient between the ablation front and the internal TPS body. The capacitive recession sensor is based on derivative capacitive sensing, whereby the capacitance decreases as the dielectric material and/or the electrodes erode with the ablated TPS material. If the dielectric material has thermal properties that make it resilient against ablation, it will remain protruded as the sandwiching electrodes are ablated. Alternatively, the simultaneous ablation of both dielectric material and electrodes can occur. SiC was selected for this first test campaign for its ablation resistance, which acted as a recession marker that measured the actual recession depth after the test. The capacitance can be expressed as:

$$C = \frac{\varepsilon[W(L-x)]}{d} \quad (1)$$

where  $\varepsilon = \varepsilon_0 \varepsilon_r$ , with  $\varepsilon_0$  being the permittivity in air (F/cm) and  $\varepsilon_r$  the dielectric constant of SiC substrate ( $\varepsilon_r=9$ , with temperature effect not considered),  $d$  is the substrate thickness (500  $\mu\text{m}$ ), and  $x$  is the ablated length of the dielectric/electrodes. The effective length,  $L$ , of the capacitor was 2.54 cm and the width,  $W$ , was 0.2 cm. Starting from the TPS forebody surface,  $x=0$ , the capacitance is at its highest initial value. During the ablation process, the effective electrode length reduces by  $L-x$ , leading to reduction in capacitance. In general, as the recession proceeds from left (refer to Fig. 2b), the capacitance would be dropping, thereby providing real-time measurement of the ablation process.

### 3. SENSOR FABRICATION AND PREPARATION

The fabrication process is summarized below. The starting substrate was a 500- $\mu\text{m}$  thick semi-insulating, single-crystal 4H-SiC. It was solvent clean with acetone, followed by isopropyl alcohol to remove organic particulates on the surface. It was followed by cleaning in 1:3 volume mixture of  $\text{H}_2\text{O}_2$  and  $\text{H}_2\text{SO}_4$ , to dissolve trace metals on the surface, followed by rinsing in de-ionized water. The wafer was then wet oxidized at 1150  $^\circ\text{C}$  for eight hours. A sputter deposition of  $\text{TaSi}_2$  (100 nm)/Pt (100 nm) was performed on front face of the wafer, followed by another 5  $\mu\text{m}$  Pt (the RTD). Other layers of  $\text{TaSi}_2$  (100 nm)/Pt (100 nm) were deposited on the 5  $\mu\text{m}$ . A 3- $\mu\text{m}$  thick Aluminum (Al) was sputtered on the top Pt. Photoresist was then spun on it and standard photolithography was performed to transfer the resistor and capacitor patterns on to the photoresist. After UV-exposure and developing of the photoresist, the Al was wet etched in phosphoric acid at 50  $^\circ\text{C}$  for 6 minutes. A second Al deposition and photolithography processes as the above were repeated, resulting in a 6  $\mu\text{m}$  thick Al mask layer. Using the thick Al as contact mask layer, the entire metallization stack in the exposed sections was etched by reactive ion etching process for six hours with the following process conditions:  $\text{Ar}=140$  sccm,  $\text{SF}_6=5$  sccm, Power=300 Wrf, Pressure=25 mT. The residual Al was subsequently dissolved in 50  $^\circ\text{C}$  phosphoric acid. On the back side of the wafer, a deposition of Ti (100 nm)/Pt (300 nm) was performed, followed by photolithography and dry etching to create the bottom recession sensor electrode. The fabrication process was completed with Ti (10 nm)/Au (500 nm) deposition and patterning to form the bond pads. Figure 3a shows the array of fabricated capacitive recession sensors and RTD's, while Fig. 3b shows the capacitive sensor diced and separated from the integrated capacitive/temperature sensors. External terminals of Au-plated Ni wires were attached to the bond pads of the capacitor and the RTD's with silver paste cured at 200  $^\circ\text{C}$ . Through-hole rectangular slits (Height= 520  $\mu\text{m}$ , Width= 0.25 cm, Depth=2.5 cm) were cut into the PICA samples by wire cutting process to receive the discrete capacitive sensors shown in Fig. 3c. A 25- $\mu\text{m}$  thick polyimide tape was wrapped around the capacitive sensor prior to sliding it into the PICA sample and mounted flush to

the ablation front (Fig. 3d). This was meant to electrically isolate the metallization of the capacitor from the PICA material to avoid the slightest electrical interference. Prior to sliding the sensors, the hole in the PICA was filled with fast setting non-electrically conductive high temperature epoxy. With the sensor slid in and flush mounted, excess epoxy that squeezed out was cleaned off, thereby securing the sensor in place and sealing the gap between the sensor and the inner walls of the PICA.

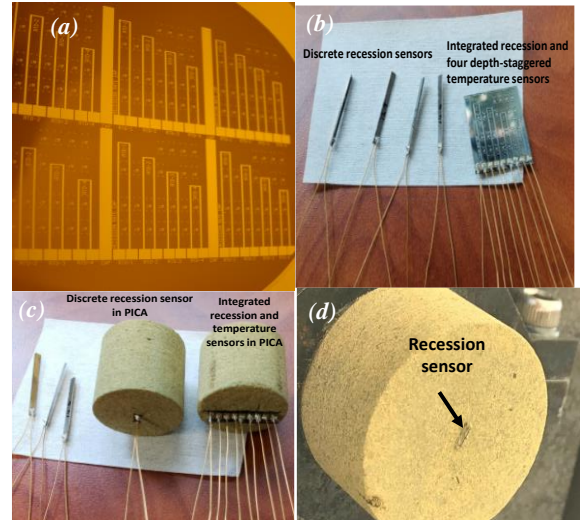


**Fig. 3: a) Wafer-level array of integrated capacitive recession and depth varied RTD's after fabrication, b) Diced and separated discrete recession sensors and the integrated recession and temperature sensors, c) Discrete recession sensor and the integrated version inserted in their respective tiny slits in PICA test articles, d) ablation front shows flush mounted recession sensor seen at the center of the PICA sample.**

### 4. TEST SETUP AND CALIBRATION

The test setup is shown in Fig. 4. The plan involved testing five PICA-embedded samples in oxy-acetylene flame at 500  $\text{W}\cdot\text{cm}^{-2}$  for 16 seconds, from which the recession sensor performance characteristics would be extracted. The recession rate sensor data was acquired using a high frequency data system at 10 kHz sampling rate. The data trigger signal was synced to the data system and LabVIEW [12]. Each PICA carrying a sensor was weighed, as well as the optical scanning of the surface topology, before and after test. The test facility uses a NI CompactRIO data system for data logging and control [12]. It was programmed to operate in Scan Interface Mode, which can only display/control data at about 1 kHz. Logging data maxes at <100 Hz but depends on the number of data channels collected. For the calibration testing, data was collected at 10 Hz and the following measurements taken were: ambient temperature, heat flux sensor cooling, water outlet temperature, solenoid actuation signal, string potentiometer signal, and heat flux sensor output voltage. Calibration of the facility was performed using a Medtherm Gardon Gauge [13], built for a range of 1000  $\text{W}\cdot\text{cm}^{-2}$ . The mixture ratio of the oxy-acetylene torch

was set using regulators from the gas bottles and metering valves downstream that were marked. Several tests were conducted, and heat flux values were repeatable. The heat flux sensor required water cooling and was nominally calibrated (by Medtherm) for 250 psig of water pressure at the inlet and outputs about 2.5 gpm. The calibration tests were performed with 150-200 psig of water pressure. A thermocouple was placed at the cooling water outlet of the heat flux sensor and data showed that with 150-200 psig of water, the water outlet temperature did not increase significantly. The torch is set to the appropriate distance (corresponding to the desired heat flux). When testing, the torch and cooling water was initiated first. The data system was then started, and the user inputs a test duration. The piston with the sample could then be actuated into the flame. If there were any safety concerns during the test, the torch could be easily shut off manually.

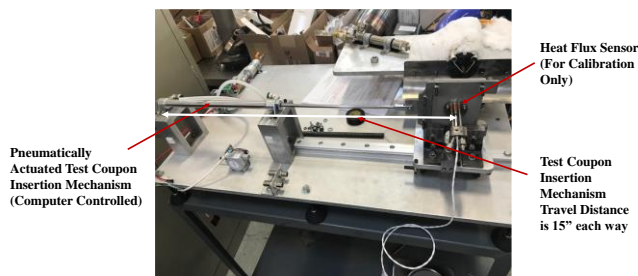


**Fig. 4: Test setup for both heat flux calibration and sensor testing.**

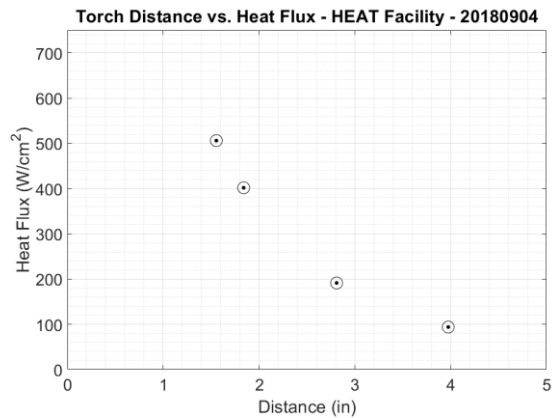


**Fig. 5: Heat flux versus distance calibration to determine optimal distance to sample that would provide 500 W-cm<sup>-2</sup> heat flux.**

The torch was set to the appropriate distance corresponding to the desired heat flux, as shown in Fig. 5 calibration chart. The rig was then calibrated to match the heat fluxes by setting heat flux sensor at different distances,  $x$ , relative to torch nozzle to create a calibration curve. A curve was fitted to the heat flux data points  $x > 1.45$  using a 3<sup>rd</sup> order polynomial and has a 0.999 R-squared value. The uncertainty of the heat flux was about from +/- 11.0 W-cm<sup>-2</sup>.

## 5. SENSOR TESTING

Only the capacitive recession sensor was tested in this first campaign. Basic metrology measurements/weighing of samples before and after test were performed. The recession sensor data was acquired with high frequency data system at 10 kHz after the capacitance was converted to voltage using a capacitance-voltage converter shown in Fig. 6 [14], where  $V_{diff}$  is the difference between output voltage  $V_{out}$  and reference voltage  $V_{ref}$  (V), and  $C_m$  and  $C_{max}$  are the measurement and maximum capacitances (F) of the sensor, respectively. The relationship between these parameters is expressed as:

$$V_{diff} = V_{out} - V_{ref} = 0.86 \frac{C_m}{C_{max}} \quad (2)$$

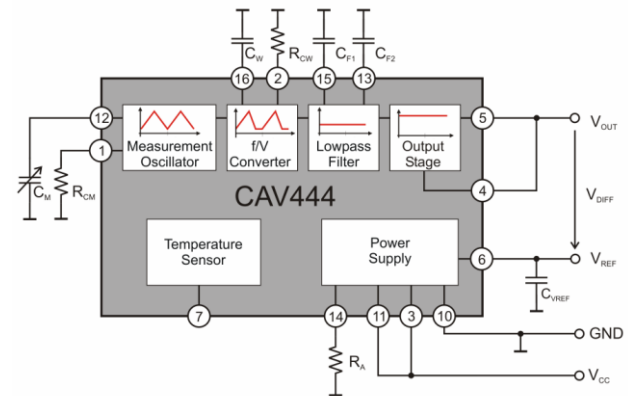


**Fig. 6: The top hierarchal schematic view of the capacitance voltage converter used during the test [14].**

The value  $C_m$  decreases during ablation, as the capacitor reduces in length or loss of electrodes. In the ideal case,  $V_{diff}$  would be visually monitored and recorded in real-time during the ablation process. It quantifies the equivalent final capacitance,  $C_m$ , from which the recession depth can be extracted as it decreases.

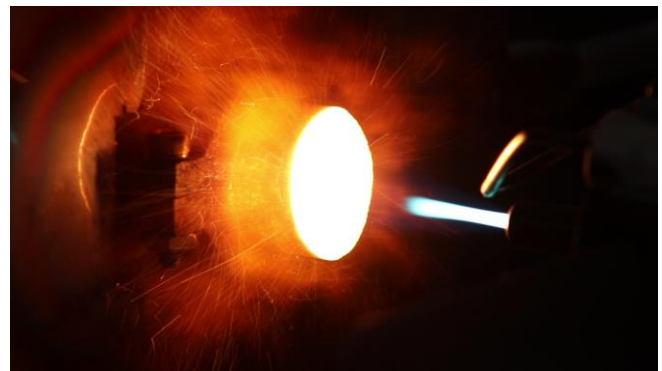


**Fig.7: Oxy-acetylene flame over the PICA and sensor.**

During testing, the torch and cooling water were initiated first. The data system was then started, and the test duration set, which in this case was 16 seconds. The piston with the sample was then actuated into the flame front after flame stabilization. Figure 7 shows the oxy-

acetylene flame impinging on the PICA and recession sensor. With the flame stabilized, the solenoid actuated the moving arm bearing the PICA sample, so that at time  $t=0$ , the PICA was in the flame front and recession data collection was then initiated.

## 6. RESULTS AND DISCUSSION

Prior to testing, line scan topological measurement of the virgin ablation of the PICA was performed with a laser across the diameter, making sure that it scanned over the recession sensor. It confirmed the sensor tip was flush mounted with the PICA surface before the test. Similar line scan was performed after each test, a representative of which is shown in Fig. 8a. The representative electrical response of the recession sensor is shown in Fig. 8, which shows voltage output  $V_{out}$  decreasing with time, as well as the differential voltage  $V_{diff}$ , which practically reached 0 V after 2.5 seconds of the 16 seconds prescribed test window. It was then observed to increase slightly at 3 s and remained constant for the rest of the test time.

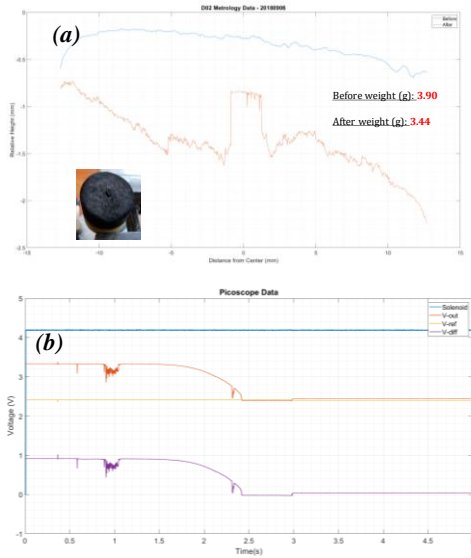


**Fig. 8:** a) Topological line scan profile of the PICA surface with the embedded recession sensor before ablation, and the profile after ablation, showing the protruding unablated recession sensor (inset), b) Recession sensor voltage output response during PICA ablation at  $500 \text{ W-cm}^{-2}$  heat flux.

This result was observed across all the five samples tested, indicating a common characteristic trend that suggested that the sensor final capacitance  $C_m$  was at the equivalent recession depth after 16 seconds. To determine the accuracy of the C-V output response, the length of the unablated SiC substrate that was protruding above the PICA char surface (Fig. 8a inset) was measured from the post-test line scan topology and shown in Table 1. Resistance to ablation of the SiC was expected, since it has a higher sublimation temperature ( $2700 \text{ }^\circ\text{C}$ ) than the oxy-acetylene flame temperature measured during the test ( $\sim 705 \text{ }^\circ\text{C}$ ). Since the SiC material did not ablate, the protruding length was initially assumed to equate the PICA recession depth to the char

surface. However, when the measured protrusion length in Table 1 was used as  $x$  in equation (1), the obtained capacitance  $C_m$  did not result in  $V_{diff}=0$ . It suggested, therefore, that the protruding bare SiC was a partial length and could not be equated to the recession depth.

**Table 2: Summary Results of  $500 \text{ W-cm}^{-2}$  Oxy-Acetylene Torch on PICA Samples with Recession Sensors.**

Sample	Initial Weight (g)	Final Weight (g)	Weight Loss (g)	Recession from Weight Loss (cm)	Sensor Tip Potrusion (cm)
D01	3.93	3.47	0.46	0.3265	0.08
D02	3.9	3.44	0.46	0.3265	0.07
D03	3.77	3.35	0.42	0.2981	0.075
D04	3.99	3.47	0.52	0.3691	0.15
D05	3.59	3.1	0.49	0.3478	0.06

The combined weight of the PICA sample, sensor, and wiring was recorded before and after each test, from which the weight loss due to ablation and charring of the PICA was determined and tabulated in Table 1. From the recorded weight loss and known  $0.28 \text{ g-cm}^{-3}$  PICA density [15], a recession depth was obtained and shown in Table 1. It is seen that the recession depth ranged between  $0.2981 \text{ cm}$  to  $0.3691 \text{ cm}$ . The summary of the test results is presented in Table 1 for the five runs at  $500 \text{ W-cm}^{-2}$ . The uncertainty in the weight measurement of the PICA samples is  $\pm 0.01 \text{ g}$ .

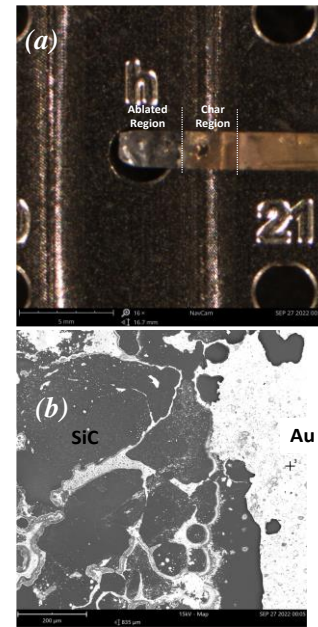


**Fig. 9:** a) Post-test optical image of the capacitive recession sensor showing the ablated (SiC), char, and unperturbed regions respectively, and b) Scanning electron microscopy image showing the bare SiC substrate section and unablated electrode (Au).

The sensor was pulled out of the PICA after the test and imaged under an optical microscope, which is shown in Fig. 9a. Three distinct boundaries are observed, one being the discontinuity between metal electrode and the bare SiC

substrate. The second region is determined to be the char region, which still retains the metal electrode, and the third region being the unperturbed PICA. Energy dispersive spectroscopy was used to analyze the sensor, which confirmed that no contiguous metallization remained on the bare SiC region while the char and unperturbed regions retained the metal electrode, as shown in Fig. 9b. It could then be confirmed that the region with missing metal electrode which extended into the char represented the actual final recession length after 16 seconds of heating. The measured length of that region was 0.325 cm (Fig. 9a), which is in good agreement with the recession depth obtained from the weight loss measurement shown in Table 1. The differences were likely due to weight loss in the char volume. These results were also in good agreement with previous work by Tran et al that exposed PICA of similar density to 805 W-cm<sup>-2</sup> heat flux for 25 seconds and obtained an average recession of 0.56 mm [16], which, by extrapolation, agreed with result obtained here. Also, Milos and Chen exposed PICA to stagnation point heat of 480 W-cm<sup>-2</sup> for 34 seconds and obtained a recession depth of 0.632 cm [17].

#### *Observations and Future Corrective Actions*

The above metrological analysis helped to explain the premature drop in  $V_{out}$  and  $V_{diff}=0$  after 2.5 s, even as the recession proceeded to completion during the 16 s test window. Post-test analysis of the C-V circuit revealed that the minimum threshold of the operating range of the capacitance,  $C_{max}$ , was about 10 pF, which turns out to be just below the initial capacitance of the sensor (10.15 pF). For the final recession length (depth) of  $x=0.325$  cm, the length of the final capacitance,  $C_{min}$ , was  $L-0.325=2.175$  cm ( $L$  being the initial length=2.54 cm). Plugging this final length, into equation (1) results in a residual capacitance of 6.93 pF, which further drops out of the circuit measurement range. In essence,  $V_{diff}$  reached zero 0 shortly into the test when the recession depth was equivalent to the lower measurement range of the circuit (10 pF). In the future, the operating range of the C-V circuit would be adjusted to have lower capacitance threshold.

Other observations were also made that would also need future corrective actions. The high thermal conductivity of the SiC substrate resulted in high heat transfer transmission to the back contact terminals of the sensor, causing overheating of the silver paste that was used to attach the Ni wires. It could have potentially compromised the electrical and mechanical integrity of the attached wire. In the future, a low thermal conductivity and high dielectric constant material would be used. The use of the silver paste to attach the external wires to the sensor bond pad would be replaced with direct Au-Au wire bonding.

## 7. CONCLUSION

The batch microfabrication of first generation integrated capacitive recession sensors and precision arranged RTD's was successfully implemented. The discrete capacitive recession sensors were successfully embedded in tiny slots cut in PICA to demonstrate ease of sensor placement while avoiding large hole drilling into the bulk TPS. This creates

opportunity for larger spatial distribution of the sensors beyond current practice. Only 2.5 seconds of real-time sensing was obtained in the prescribed window of 16 seconds. This was due to the decreasing capacitance dropping out of the measurement range of the C-V circuit before end of test. Post-test evaluation, however, confirmed that the recession depths obtained were in good agreement with previously published results. The lessons learned from this initial test campaign would be used to improve sensor performance in the future.

## ACKNOWLEDGEMENTS

This work was funded under the Center Innovation Fund of the National Aeronautics and Space Administration (NASA). Supplemental funding was provided by the NASA Orion Mission-2 Project. The first author thanks Ed Martinez and Dr. Mairead Stackpoole of NASA Ames Research Center for providing the PICA samples.

## REFERENCES

- [1] Lillard, R., Olejniczak, A., "Human Mars EDL pathfinder study: Assessment of technology development gaps and mitigations," 2017 IEEE Aerospace Conference, Big Sky, Montana, USA, 04-11 March 2017. DOI: 10.1109/AERO.2017.7943587. 2017.
- [2] Skolnik, N., Kamezawa, H., Li, L., Rossman, G., Sforzo, B., Braun, R.D., "Design of a Novel Hypersonic Inflatable Aerodynamic Decelerator for Mars Entry, Descent, and Landing," AIAA Atmospheric Flight Mechanics Conference, AIAA SciTech Forum, (AIAA 2017-0469).
- [3] Salotti, J.-M., "Robust, affordable, semi-direct Mars mission." *Acta Astronautica* **127**, 235-248. 2016.
- [4] Braun, R.D., Manning, R., "Mars Exploration Entry, Descent, and Landing Challenges," *Journal of Spacecraft and Rockets*, Vol. 44, No. 2, pp. 310-323. 2007.
- [5] Hwang, H.H., Bose, D., et al., "Mars 2020 Entry, Descent and Landing Instrumentation 2 (MEDLI2)," 46<sup>th</sup> AIAA Thermophysics Conference, 13-17 June 2016, Washington, D.C.
- [6] Wright, M.J., Bose, D., Chen, Y.-K., "Probabilistic Modeling of Aerothermal and Thermal Protection Material Response Uncertainties," *AIAA Journal* Vol. 45, No. 2, pp. 399. 2007.
- [7] Wright, M.J., Tang, C. Y., Edquist, K.T., Hollis, B.R., Krasa, P., Campbell, C.A., "A Review of Aerothermal Modeling for Mars Entry Missions," AIAA 2010-0443.
- [8] Santos, J. A. B, Edquist, K. T., Hwang, H. H. 2023-2032 Decadal Survey White Paper: Entry, Descent, and Landing Instrumentation. 2020.
- [9] Noffz and Bowman et al had used two-wire capacitance based recession sensor for sensing ablation [NASA Technical Memorandum 4777, 1996.
- [10] Cassanto J. M., Droms C. R., Metzger J., "Simple Recession Gage for In-flight Measurement of the Char Degradation Zone for Re-Entry Vehicle Heat Shields, 26th International Instrumentation Symposium, Seattle,

WA, USA. 1980.

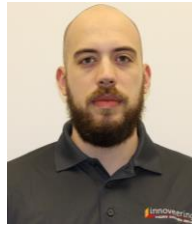
- [11] Papadopoulos, G, Tiliakos, N., Benel, G., Thomson, C., "Non-Intrusive Sensor for in-situ Measurement of Recession Rate of Heat Shield Ablatives," AIAA Infotech@Aerospace 2010 20-22 April 2010, Atlanta, Georgia.
- [12] <https://www.ni.com/en-us/shop/labview.html>
- [13] <https://medtherm.com/>
- [14] <https://www.analog-micro.com/>
- [15] <https://ntrs.nasa.gov/citations/20110014590>
- [16] Tran et. al, "Phenolic Impregnated Carbon Ablators (PICA) as Thermal Protection Systems for Discovery Missions," 31st AIAA Thermophysics Conference, New Orleans, LA, June 17-20, 1996.
- [17] Milos, F.S., Chen, Y.-K, "Ablation and Thermal Response Property Model Validation for Phenolic Impregnated Carbon Ablator," AIAA-2009-0262. 2009.

## BIOGRAPHY



**Robert Okojie** received the BS, MS and Ph.D. degrees in Electrical Engineering from the New Jersey Institute of Technology, Newark, New Jersey, between 1991 and 1996. He was a Senior Research Scientist at Kulite Semiconductor Products, Inc., Leonia, NJ, from 1993 to 1997, developing high

temperature ohmic contacts to SiC semiconductor pressure sensors for high temperature applications. He became a Senior Research Engineer at Ford Microelectronics, Colorado Springs, CO, in 1997, developing MEMS-based sensors, smart fuel injectors, and associated packaging technologies. In August 1999, he joined the SiC research group at NASA Glenn Research Center, Cleveland OH, as an Electronics Engineer, developing enabling technologies for SiC microsystems for extreme environments. He had served as the Associate Project Investigator in Hypersonic Project Experimental Capabilities of the NASA Fundamental Aeronautics Program. He was inducted into the NASA Inventors Hall of Fame in 2020; received the 2012 NASA Glenn Research Center Distinguished Publication Award in 2012; in 2009, the Abe Silverstein Medal for Research, and numerous other awards between 2002 and 2018. He is a Senior Member of the IEEE and member and published over 50 peer reviewed papers in scientific journals and conference proceedings relating to high temperature MEMS technology, and a contributing author to the CRC MEMS Handbook. He has mentored over 20 student interns since joining the Agency and holds over 20 US patents.



**Christian Petrov** received his B.S. in Mechanical Engineering from the City College of New York in 2016 and has worked with Innoveering since graduation. Christian has been involved in areas ranging from design, test and analysis of multiple sensor developments, as well the early

and ongoing development of Innoveering's testing infrastructure. This includes design and test development for the Innoveering's Mach 2 and Mach 4 tunnels and their associated test efforts. He has also lead design activities in conjunction with other external test facilities and research labs. Christian led the effort for the test methodology and execution on Innoveering's side for the Minimally Intrusive Single-Chip Recession/ Temperature Sensors work with Dr. Robert Okojie.

**Gary Go** is the lead design engineer/design manager at Innoveering for the past 5 years, where he leads the design of various test facilities and test articles for hypersonic applications. He was a key member in designing/developing/testing a low-speed combustor for a large aerospace firm. This included implementing a gas-sampling system to measure in-flame gas constituents and temperatures. He led the design of a gas-sampling rake for a high speed, high enthalpy blowdown facility. Gary also has experience in setting up data acquisition systems and programming data processing/analysis tools. Gary obtained his BS/MS in Mechanical Engineering from Cooper Union in NYC.



**Nicholas Tiliakos** has 25 years of professional engineering experience that includes 16.5 years (1997-2013) at ATK GASL (now Northrop Grumman), as Senior R&D Engineer and 9.5 years at Innoveering (2013-present), formerly as Chief Technologist now

as V.P. of Science & Technology. His responsibilities include program management, engineering, to business development. He has a varied experience base ranging from: development/testing of advanced hypersonic propulsion systems, aero-thermodynamics/thermal fluids/engine performance analysis, aero-propulsion/rocket engine/combustion systems testing, MEMS, and harsh environment sensors development. Currently, he is working to develop advanced materials test techniques/diagnostics. Nicholas obtained his BS in Mechanical Engineering from Cornell University (1990) and his MS/PhD in Aerospace Engineering from the University of Illinois @ Urbana-Champaign (1997).